Journal of The Electrochemical Society, **153** (1) H4-H14 (2006)
0013-4651/2005/153(1)/H4/11/$20.00 © The Electrochemical Society, Inc.

Mixed Ionic and Electronic Conduction in Li_3PO_4 Electrolyte for a CO_2 Gas Sensor

Chonghoon Lee,[a,*] Prabir K. Dutta,[b] Ramasamy Ramamoorthy,[b,c] and Sheikh A. Akbar[,a,z]**

Center for Industrial Sensors and Measurements, The Ohio State University, Columbus, Ohio 43210, USA

An electrochemical CO_2 gas sensor using Li_2CO_3 and $Li_2TiO_3 + TiO_2$ as sensing and reference electrodes, respectively, and Li_3PO_4 as the electrolyte is the subject of this paper. The sensor response to CO_2 gas showed a systematic deviation from the prediction of the Nernst equation at low p_{CO_2}. Based on the electromotive force (emf) measurement, the transference numbers of Li_3PO_4, a lithium-ion conductor, were estimated for different p_{CO_2} values, and the conduction domain boundary for Li_3PO_4 separating n-type electronic conduction from ionic conduction was constructed. The conduction domain predicts that change in the Li activity in the sensing side of the cell drives the Li_3PO_4 electrolyte to a mixed (n-type electronic and ionic) conduction region at low p_{CO_2}. Hebb-Wagner dc polarization measurements also indicate n-type electronic conduction in Li_3PO_4 with a mixture of Li_2CO_3 and gold as a reversible electrode. The transference numbers obtained from both the emf measurement and the Hebb-Wagner polarization measurements demonstrate that the origin of the non-Nernstian behavior of the CO_2 sensor is due to the lithium mass transport from the Li_2CO_3-sensing electrode to the Li_3PO_4 electrolyte, resulting in nonstoichiometry of Li_3PO_4 at temperatures above 500°C.
 [DOI: 10.1149/1.2129180]

Manuscript submitted July 12, 2005; revised manuscript received August 17, 2005. Available electronically November 23, 2005.

Electrochemical CO_2 gas sensors exhibit good selectivity, sensitivity, and stability.[1-5] Electrochemical sensors, especially equilibrium potential types, are most promising for CO_2 monitoring among the solid-state-based technologies. Equilibrium potential sensors have been generally classified into three broad groups.[1-3] The type-III design, also called a surface-modified sensor, is attractive for CO_2 sensing because it offers flexibility in terms of designing the sensor with different auxiliary materials and electrolytes.

Extensive studies of CO_2 gas sensors have focused on sodium-ion conductors such as Nasicon and Na-β-alumina.[6-9] However, alkali-metal-based sensors are sensitive to humidity and deteriorate the sensing performance.[8] Lithium compounds are known to be more resistive to humidity than other alkali metal compounds. Previous studies by the authors[10,11] on CO_2 sensors with $Li_{2.88}PO_{3.73}N_{0.14}$ and Li_3PO_4 electrolytes and Li_2CO_3 sensing electrodes have demonstrated excellent CO_2 sensing performance in the laboratory as well as in automobile exhaust.[12,13] Moreover, Na-ion conductors are not compatible with microelectronic fabrication technology for integration of several sensors into electronic chips and mass production for commercialization. Because Li_3PO_4 electrolyte has been fabricated as a Lipon glass thin film in battery applications,[14-16] it is a potential electrolyte candidate for thin-film CO_2 gas sensors.

Non-Nernstian sensor response has been often reported in literature,[17-19] which uses Na-ion-conducting potentiometric cells. Sadaoka et al.[17] claimed that the number of electrons in the electrochemical reaction of Na_2CO_3 auxiliary phase is higher than two and is responsible for the slope change in the Nernst equation. Alonso-Porta and Kumar[18] suggested that Na_2CO_3 is not stable in contact with Nasicon electrolyte, resulting in a thin Na_2O layer at the interface that can affect the number of electrons involved in the electrochemical reaction of Na_2CO_3. Ramirez-Salgado et al.[19] pointed out that the overpotential due to the slow charge transfer and CO_2 diffusion in the Na_2CO_3 sensing electrode are responsible for the non-Nernstian behavior. The formation of Na_2O layers or sluggish kinetics of Na_2CO_3 electrochemical reaction can induce mixed potential instead of equilibrium potential, and the Nernst equation is not valid for the prediction of electromotive force (emf). In this study, we demonstrate that the electronic conductivity of the Li_3PO_4 electrolyte is responsible for the deviation from the Nernst equation by using transference number based on emf and Hebb-Wagner polarization measurements.

Experimental

Li_3PO_4 sample preparation and characterization.— Lithium phosphate, Li_3PO_4, with 5 mol % SiO_2 additive was used as the electrolyte in this study. Li_3PO_4 (99.5%) and SiO_2 (99.5%) obtained from Alfa Aesar were ballmilled in isopropanol for 8 h and dried at 120°C. The dried powder mixture was cold pressed into pellets of 8 mm diam and sintered at 800°C for 8 h with a heating/cooling rate of 2°C/min. Sample geometry with diameter 0.76 cm and thickness 0.12 cm was used for all the electrical measurements. X-ray diffraction (XRD) was used for phase identification. The data were collected in the 2θ range of 20–80° with a Scintag XDS 2000 X-ray diffractometer using Cu Kα radiation at 45 kV and 20-mA current. Scanning electron microscopy (SEM) was performed using a Philips XL30 ESEM.

Sample preparation for total conductivity measurement.— The total conductivity was measured using gold ion-blocking electrodes. A CrC-150 Torr International, Inc., sputtering system and gold target (99.99% purity, 3-in. diam × 0.5 mm thick, Sputteringmaterials, Inc.) were used. The sputtering was performed in an Ar gas (working pressure 4.5×10^{-3} Torr) for 10 min to get a fully dense film on top of the electrolyte. After the sputtering of gold, the sample was annealed at 700°C for 5 h with a 5°C/min heating/cooling rate. Gold wire was attached using gold paste. It was cured at 700°C for 1 h with a 5°C/min heating/cooling rate.

Sample preparation for emf measurement.— The structure and design of the electrochemical cell for the emf measurement, a CO_2 sensor with Li_2CO_3 and Li_2TiO_3 electrodes, is described elsewhere.[11] Porous gold electrode structure was obtained using the sputtering process. Sputtering time was set from 4.5 to 7.5 min for optimum porosity. A postannealing at 700°C for 5 h with a 5°C/min heating/cooling rate provided a porous gold electrode morphology on Li_3PO_4.

Li_2TiO_3 (Lithium Corporation of America, Inc.) mixed with 5 mol% TiO_2 (Alfa Aesar, 99.9%) was used as the reference electrode. The powder mixture was ballmilled in ethanol for 8 h and then mixed with α-terpineol organic binder (Fisher Chemicals) and

* Electrochemical Society Student Member.
** Electrochemical Society Active Member.
[a] Present address: Department of Materials Science and Engineering, The Ohio State University, Columbus, Ohio 43210-1178, USA.
[b] Present address: Department of Chemistry, The Ohio State University, Columbus, Ohio 43210-1302, USA.
[c] On leave from GE Advanced Materials, Strongsville, Ohio 44149, USA.
[z] E-mail: Akbar.1@osu.edu

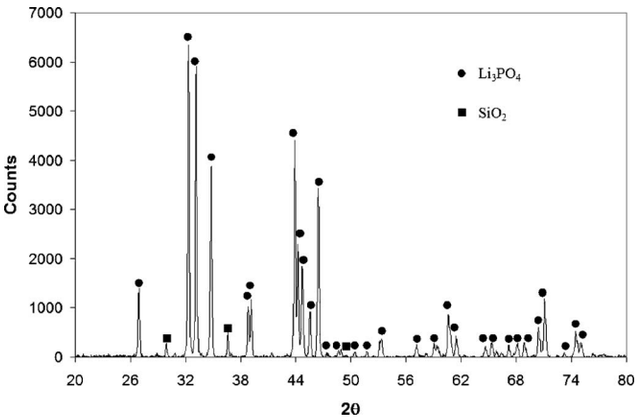

Figure 1. XRD pattern of Li_3PO_4 + SiO_2 (5 mol %) after sintering for 8 h at 800°C.

painted on the porous gold electrode. It was cured at 700°C for 1 h. Li_2CO_3 (Alpha Aesar, 99.999%) was used as the sensing electrode. It was also mixed with α-terpineol and painted on gold electrode on the other side by hand-painting and was heat-treated at 600°C for 1 h.

Sample preparation for Hebb-Wagner polarization measurement.— Hebb-Wagner polarization measurement requires one reversible electrode and the other to be an ion-blocking electrode. Gold paste (Heraeus gold ink) was used for the ion-blocking electrode. A thick gold paste was applied and cured at 700°C for 1 h at a heating/cooling rate of 5°C/min. On the other side of the pellet, a reversible electrode was made from lithium carbonate and gold paste mixture. This electrode was cured at 600°C for 1 h.

Gas preparation and electrical measurements.— Three gas species (N_2, air, and CO_2) were mixed in appropriate proportions to get different concentrations of CO_2 from 500 ppm to 50%. A mixture of ultrahigh-purity nitrogen and synthetic air was used as a background gas in all measurements, flown at a rate of 210 mL/min. A schematic of the test assembly is given elsewhere.[20] The tests were performed at temperatures ranging from 400 to 600°C. A Solartron 1260 impedance analyzer was used to measure the total conductivity of the electrolyte. The frequency was swept from 0.01 Hz to 10 MHz. The emf was measured by an HP 34970A voltmeter which

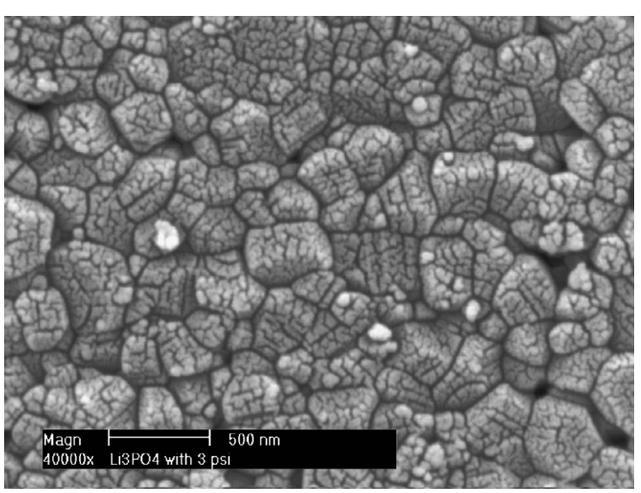

Figure 2. SEM micrograph of Li_3PO_4 + SiO_2 (5 mol %) after sintering for 8 h at 800°C.

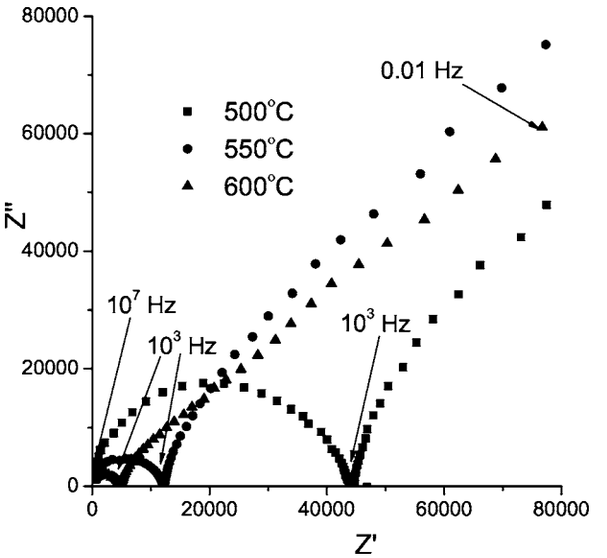

Figure 3. Impedance plot of gold-ion-blocking electrode for Li_3PO_4 at 500, 550, and 600°C.

was interfaced with a computer using the HP Benchlink data logger software for data acquisition. A Gamry PC4/300 instrument was used to measure the steady-state current in the potentiostatic mode. Potential was increased in 0.05- or 0.1-V steps from 0.05 to 1.4 V. Each step was maintained for 2 h to collect the steady-state current data.

Results

Phase of Li_3PO_4 electrolyte and its total conductivity.— The powder XRD pattern of sintered Li_3PO_4 with 5 mol % SiO_2 is shown in Fig. 1, indicating a two-phase mixture even after sintering. The SiO_2 addition only helps mechanical stability of the electrolyte. Figure 2 shows the SEM picture of the fairly dense surface of the lithium phosphate electrolyte.

The total conductivity was measured using gold ion-blocking electrodes. Figure 3 shows a typical impedance spectra using gold ion-blocking electrodes swept from 10^7 to 0.01 Hz in air at 500, 550, and 600°C. The depressed semicircle in the high-frequency region represents a distribution of the relaxation frequencies which correspond to bulk and grain boundary contributions. The total ionic

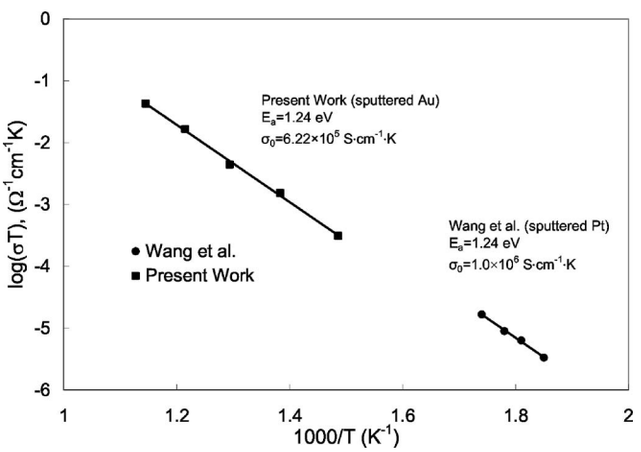

Figure 4. Arrhenius plot of the total conductivity of Li_3PO_4 electrolyte with gold-ion-blocking electrode.

Table I. Measured resistance, and calculated conductivity and transference number from impedance measurement and dc measurement.

			R_e (Ω)			
	R_T (Ω)	σ_T (Ω^{-1} cm^{-1})	DC	Fitting	σ_e (Ω^{-1} cm^{-1})	t_i
400°C	5.53×10^5	4.59×10^{-7}	1.20×10^7	6.22×10^6	2.11×10^{-8}	0.95
450°C	1.20×10^5	2.11×10^{-6}	5.59×10^6	3.13×10^6	4.54×10^{-8}	0.98
500°C	4.44×10^4	5.70×10^{-6}	2.16×10^6	1.64×10^6	1.18×10^{-7}	0.98
550°C	1.27×10^4	1.99×10^{-5}	1.18×10^6	1.13×10^6	2.15×10^{-7}	0.99
600°C	5.19×10^3	4.89×10^{-5}	4.29×10^5	4.29×10^5	5.90×10^{-7}	0.99

and electronic conductivity of Li_3PO_4 was obtained from the high-frequency semicircle because the impedance of ion-blocking electrode capacitance component is negligible at high frequency. The low-frequency semicircle was not fully represented in the tested frequency range. The electronic conductivity of Li_3PO_4 was calculated by fitting the low-frequency semicircle. At low frequency, the ion-blocking electrode can totally block the ionic conductivity and allow only electronic conductivity. In order to confirm the fit, dc measurements were performed and they agree well with the values obtained from the low-frequency semicircle. The total and electronic conductivity values from impedance measurement at various temperatures are shown in Table I. The resistance of the second semicircle is larger than the first semicircle by about 2 orders of magnitude. It shows that the total conductivity of Li_3PO_4 is almost equivalent to the ionic conductivity. This implies that lithium phosphate is almost a pure ionic conductor when it is attached to an ion-blocking electrode. Impedance measurement for the transference number is discussed later in detail.

The ionic conductivity (σ) data is plotted as $\log(\sigma T)$ vs reciprocal temperature ($1000/T$) in Fig. 4. The data shows a good fit to the Arrhenius equation

$$\sigma T = \sigma_0 \exp\left(-\frac{E_a}{kT}\right) \quad [1]$$

$$\log \sigma T = \log \sigma_0 - 0.434\frac{E_a}{1000k}(1000/T) \quad [2]$$

where E_a is the activation energy for the ionic conductivity, σ_0 the pre-exponential constant, and k the Boltzmann constant (8.62×10^{-5} eV/K). The activation energy of 1.24 eV for the ionic conduction from Eq. 2 agrees well with literature[21,22] as shown in Table II, though there is a difference in σ_0.

EMF measurement.— The emf values were measured for CO_2 concentrations ranging from 500 ppm to 50% at temperatures from 400 to 600°C with the cell

$$O_2, CO_2, (Li_2TiO_3 + TiO_2, Au) \overset{I}{|} \underset{a'_{Li}}{Li_3PO_4} \overset{II}{|} (Au, Li_2CO_3), CO_2, O_2 \quad [3]$$

Following the Nernst equation, the measured emf of the above cell is given by

$$\text{emf} = -\frac{\Delta G}{nF} = -\frac{(\mu^o_{Li_2CO_3} + \mu^o_{TiO_2} - \mu^o_{Li_2TiO_3} - \mu^o_{CO_2})}{2F} + \frac{RT}{2F}\ln p_{CO_2} \quad [4]$$

where $\mu^o_{Li_2CO_3}$, $\mu^o_{TiO_2}$, $\mu^o_{Li_2TiO_3}$, and $\mu^o_{CO_2}$ are the standard state molar Gibbs free energies of formation of Li_2CO_3, TiO_2, Li_2TiO_3, and CO_2, respectively. These values are found in Ref. 23 and shown in Table III. R is the gas constant, F the Faraday constant, T the absolute temperature, and p_{CO_2} the partial pressure of CO_2. Figure 5 shows the temperature dependence of measured emf of this cell at different CO_2 concentrations. Straight lines are the Nernst emf calculated from Eq. 4. It shows that the measured emf does not coincide with the theoretical prediction. Closest match between theory and experiment occurs at around 500°C, which lies in the middle of the tested temperature range.

The cell emf can also be represented as a function of the lithium activity in Li_2CO_3 sensing electrode under thermodynamic equilibrium instead of CO_2 partial pressure because lithium activity was calculated from Eq. B-4 shown in Appendix B. The emf values as a function of lithium activity, a''_{Li}, at 500 and 600°C are plotted in Fig. 6 and 7, respectively. The sensor shows different sensitivity under low CO_2 (high a''_{Li}) and high CO_2 (low a''_{Li}) concentrations at both 500 and 600°C. The sensitivity for lower concentrations (500–5000 ppm) is found smaller than that for high (5–50%) concentrations. Therefore, it is clear that cell 3 does not follow the Nernst equation, and its emf systematically deviates from the theoretically calculated values.

The non-Nernstian behavior can be interpreted by using the Wagner cell voltage equation (Eq. 5), which is generally used for a cell with mixed ionic and electronic conductor (MIEC)

$$\text{emf} = -\frac{RT}{F}\left[\ln\frac{a_\oplus + a''_{Li}}{a_\oplus + a'_{Li}} + \ln\frac{a_\ominus + a'_{Li}}{a_\ominus + a''_{Li}}\right] \quad [5]$$

where a'_{Li} is the lithium activity in the reference electrode, a''_{Li} in the sensing electrode, $a_\ominus$ the electron conduction parameter, and $a_\oplus$ the hole conduction parameter.[24-27] The derivation of this equation is based on Eq. 28, shown later. Considering the lithium activities in the sensing and the reference electrode calculated from Table III,

Table II. Comparison of E_a and σ_0 for Li_3PO_4 electrolyte of the present study and literature reported values.

	E_a (eV)	σ_0 (S cm^{-1} K)
Present study	1.24	6.22×10^5
Wang et al.[21] (J. Solid State Chem. 1995)	1.24	1.0×10^6
Hu et al.[22] (J. Electrochem. Soc. 1977)	1.30	2.5×10^6

Table III. Standard formation energy of Li_2CO_3, TiO_2, Li_2TiO_3, and CO_2 at different temperatures.[23]

Temp (K)	$\Delta_f G^o_{(Li_2CO_3)}$ (J/mol)	$\Delta_f G^o_{(TiO_2)}$ (J/mol)	$\Delta_f G^o_{(Li_2TiO_3)}$ (J/mol)	$\Delta_f G^o_{(CO_2)}$ (J/mol)
600	−1045224	−822753	−1485520	−395182
673	−1024180	−814579	−1462299	−395340
700	−1016366	−809706	−1453710	−395398
723	−1009917	−805600	−1446424	−395441
773	−995831	−796642	−1430584	−395535
800	−988225	−791810	−1422030	−395586
823	−981833	−787724	−1414775	−395623
873	−967938	−778842	−1399004	−395704
900	−960434	−774046	−1390488	−395748

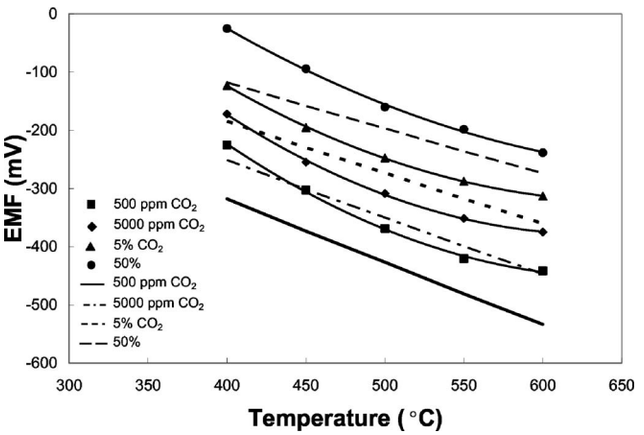

Figure 5. The emf of the sensor as a function of temperature for various CO_2 partial pressures.

there are two possibilities for the electrolyte. In the case ($a_{\oplus} \ll a'_{Li} < a''_{Li}$), Eq. 5 can be simplified to

$$\text{emf} = -\frac{RT}{F}\left[\ln \frac{a''_{Li}(a_{\ominus} + a'_{Li})}{a'_{Li}(a_{\ominus} + a''_{Li})}\right] \quad [6]$$

In the case ($a'_{Li} < a''_{Li} \ll a_{\ominus}$), Eq. 5 is reduced to

$$\text{emf} = -\frac{RT}{F}\left[\ln \frac{(a_{\oplus} + a''_{Li})}{(a_{\oplus} + a'_{Li})}\right] \quad [7]$$

Equation 6 implies electron conduction is prevalent in the MIEC, whereas Eq. 7 represents hole conduction. These equations allow us to calculate electron conduction parameter $a_{\ominus}$ or hole conduction parameter $a_{\oplus}$. Both equations were used to fit the measured emf vs a''_{Li} by using Origin 7.0 software, and the lithium activity a'_{Li} and the conduction parameter $a_{\ominus}$ or $a_{\oplus}$ were used as fitting parameters. Equation 6 provides a better fit to the measured emf at 500 and 600°C. The $a_{\ominus}$ and a'_{Li} derived from the curve fitting are shown in Table IV.

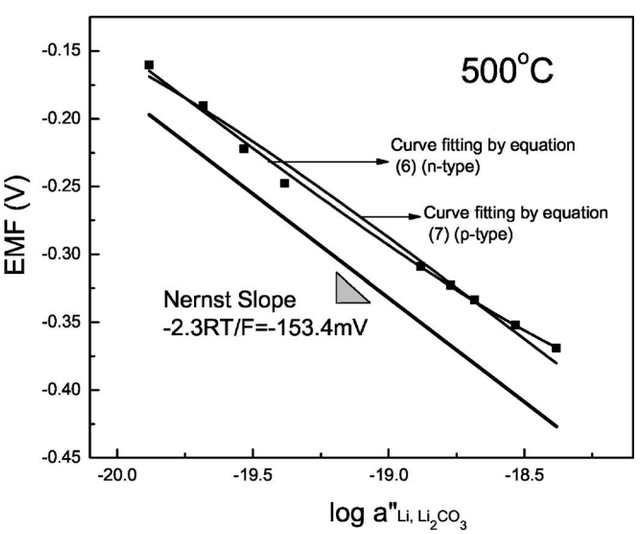

Figure 6. The measured and the theoretical emf of the sensor as a function of $\log a''_{Li}$ in Li_2CO_3 for various CO_2 partial pressures at 500°C.

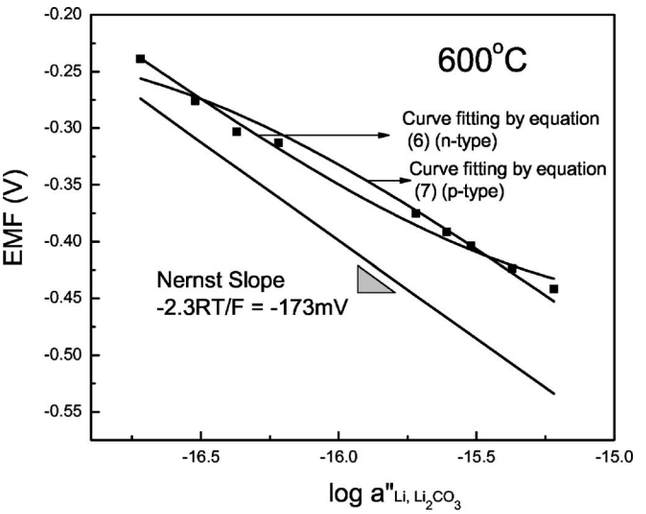

Figure 7. The measured and the theoretical emf of the sensor as a function of $\log a''_{Li}$ in Li_2CO_3 for various CO_2 partial pressures at 600°C.

Hebb-Wagner polarization measurement.— For the Hebb-Wagner polarization measurement, the following cell with Li_3PO_4 was constructed

$$\ominus Li_2CO_3 + \text{Au (mixture)}|Li_3PO_4 + 5 \text{ mol \% } SiO_2|\text{Au (ion-blocking electrode)} \oplus \quad [8]$$

Li_2CO_3 + gold electrode was used as a reversible electrode in this experiment. The test gas composition was chosen to be 500 ppm CO_2 and 10% O_2 in balance N_2. An open-circuit potential of −374 mV was measured at 500°C before applying the external voltage. Figure 8 shows typical current vs time at applied potentials from 0.05 to 1.4 V at 500°C. Measured current density values with respect to applied voltage are shown in Table V. The response at early times was faster followed by a slower change in current. The current curves were monitored for 2 h at each voltage and they were fitted by an exponential decay function (Eq. 9) to find the steady-state current values from I_0

$$I(t) = A_1 \exp\left(-\frac{t}{t_1}\right) + A_2 \exp\left(-\frac{t}{t_2}\right) + A_3 \exp\left(-\frac{t}{t_3}\right) + I_0 \quad [9]$$

Figure 9 presents the plot of the steady-state current density vs the potential at 500°C. A current plateau in the range of 0.3–0.9 V and a subsequent fast increase of the current are seen. When the sample is polarized with ion-blocking electrodes, electronic current density in a one-dimensional case is given by

$$J = \left\{\sigma_n\left[1 - \exp\left(-\frac{EF}{RT}\right)\right] + \sigma_p\left[\exp\left(\frac{EF}{RT}\right) - 1\right]\right\}\left(\frac{RT}{RL}\right) \quad [10]$$

where σ_n and σ_p are the conductivity due to electrons and holes, respectively, and L is the sample thickness.[28] σ_n and σ_p are obtained from fitting the data in Fig. 9 by using Eq. 10 and the values are estimated to be

Table IV. Calculated $a_{\ominus}$ and a'_{Li} from the curve fitting with Eq. 6.

Temp (°C)	R^2	$a_{\ominus}$	a'_{Li}
500	0.9965	8.24×10^{-19}	1.09×10^{-21}
550	0.9979	3.73×10^{-17}	3.55×10^{-20}
600	0.9917	3.87×10^{-16}	7.58×10^{-19}

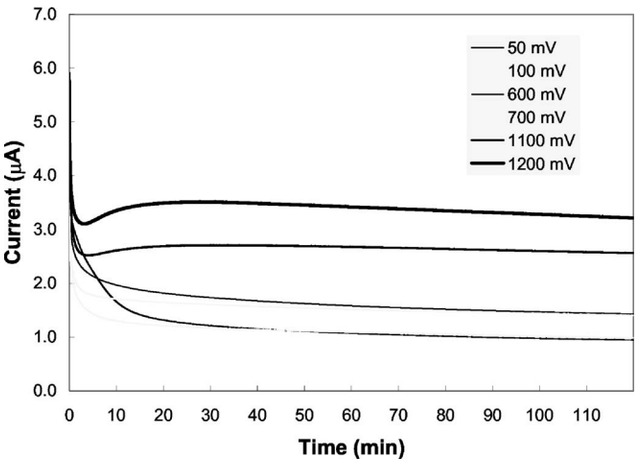

Figure 8. A typical time response of the current in Hebb-Wagner measurement for Li_3PO_4 at 500°C.

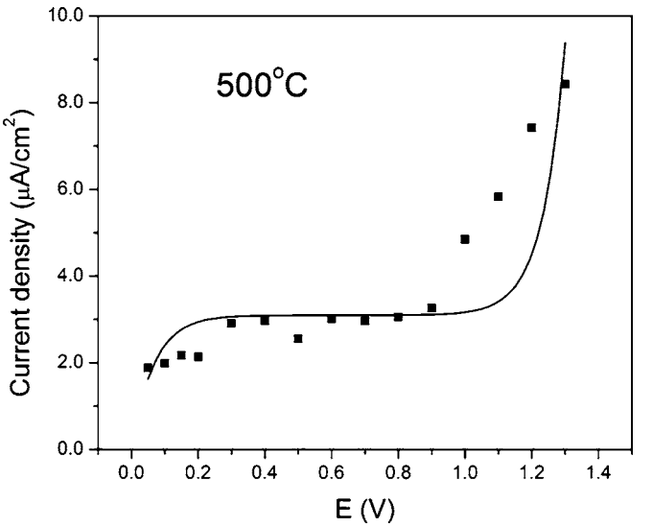

Figure 9. Hebb-Wagner polarization curve for Li_3PO_4; steady-state current as a function of the applied voltage at 500°C.

$$\sigma_n = 5.34 \times 10^{-6}\ \Omega^{-1}\ cm^{-1}$$

$$\sigma_p = 3.62 \times 10^{-14}\ \Omega^{-1}\ cm^{-1}$$

This result indicates that σ_n is much higher than σ_p in Li_3PO_4 when it is in contact with Li_2CO_3 reversible electrode. Similar observations were also found at 600°C. The ideal I–V relations are not observed at 600°C by fitting the data, but the electronic conductivity can be extracted relying on the plateau current.

Discussion

The important requirements for equilibrium potential sensors are (*i*) reversible electrode reactions and (*ii*) pure ion-conducting properties of the electrolyte. A reversible electrode is an electrode that establishes thermodynamic equilibrium potential when oxidation and reduction currents are balanced on the electrode. Nernst equation for CO_2 sensor cell is derived from these two unconditional assumptions. The ideal behavior of CO_2 sensor cells with a perfect lithium-ion conductor following the Nernst equation can be understood from the schematic of electrochemical, chemical, and electrical potential profiles shown in Fig. 10. The electrochemical potentials are located at the highest level to indicate that they are the sum of both the chemical and the electrical potentials. The solid lines represent fixed potentials in this system and broken lines are the variable potentials. Chemical potential of oxygen is a variable, but both sides have the same oxygen partial pressure so it does not appear in the overall electrochemical equilibrium. Fixed chemical potential of lithium carbonate, titania, and lithium titanate are located in the order of their standard state chemical potentials. The electrochemical potential of lithium ions is equilibrated ($\Delta\tilde{\mu}_{Li^+} = 0$) via three different phases, but the electrochemical potential of the electrons in the two gold electrodes is not equilibrated ($\Delta\tilde{\mu}_{e^-} \neq 0$), because the Li_3PO_4 is assumed to be a perfect ionic conductor in this model. The overall emf is dependent only on the CO_2 partial pressure, as can be seen in Eq. 4 under thermodynamic equilibrium. Therefore, if slow electrochemical reactions at the electrodes hinder the establishment of the thermodynamic equilibrium, then the equilibrium potential is not achieved. However, in this case, the deviation from the Nernst equation should gradually decrease with increasing sensor operating temperature. More detailed discussion about this ideal model for the type-III sensor is found elsewhere.[20,24]

The Nernst equation (Eq. 4) can also be represented in terms of Li activities at the electrodes under thermodynamic equilibrium. The emf is dependent on the lithium chemical potential difference between the reference and the sensing electrodes

Table V. Applied voltage vs steady-state current density values from Hebb-Wagner method at 500°C.

Applied voltage (V)	Current density ($\mu A/cm^2$)
0.05	1.88×10^{-6}
0.01	1.99×10^{-6}
0.15	2.17×10^{-6}
0.2	2.14×10^{-6}
0.3	2.91×10^{-6}
0.4	2.97×10^{-6}
0.5	2.55×10^{-6}
0.6	3.01×10^{-6}
0.7	2.96×10^{-6}
0.8	3.06×10^{-6}
0.9	3.26×10^{-6}
1	4.85×10^{-6}
1.1	5.83×10^{-6}
1.2	7.42×10^{-6}
1.3	8.43×10^{-6}

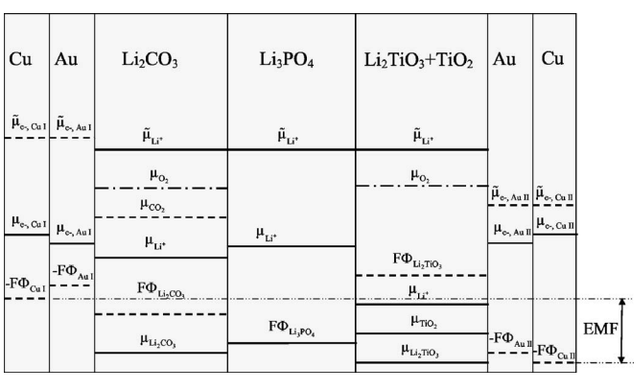

Figure 10. Schematic profile of electrochemical, chemical, and electrical potentials for the CO_2 sensor cell in thermodynamic equilibrium for the case of a pure ionic conductor.

Table VI. Calculated lithium activity at the Li_2CO_3, sensing electrode, and measured emf under various CO_2 concentrations at 500 and 600°C.

	500°C		600°C	
CO_2 concentration	a''_{Li}	emf (V)	a''_{Li}	emf (V)
500 ppm	4.15×10^{-19}	−0.369	6.03×10^{-16}	−0.442
1000 ppm	2.93×10^{-19}	−0.352	4.27×10^{-16}	−0.424
2000 ppm	2.07×10^{-19}	−0.333	3.02×10^{-16}	−0.404
3000 ppm	1.69×10^{-19}	−0.323	2.46×10^{-16}	−0.392
5000 ppm	1.31×10^{-19}	−0.309	1.91×10^{-16}	−0.375
5%	4.15×10^{-20}	−0.248	6.03×10^{-17}	−0.313
10%	2.93×10^{-20}	−0.222	4.27×10^{-17}	−0.303
20%	2.07×10^{-20}	−0.190	3.02×10^{-17}	−0.276
50%	1.31×10^{-20}	−0.160	1.91×10^{-17}	−0.239

$$\text{emf} = -\frac{RT}{F}\ln\left(\frac{a''_{Li}}{a'_{Li}}\right) \quad [11]$$

a'_{Li} can be calculated from the equilibrium reaction of the reference electrode

$$Li_2TiO_3 = 2Li + TiO_2 + \frac{1}{2}O_2 \quad [12]$$

This reaction is thermodynamically independent of CO_2 partial pressure and in this experiment the oxygen partial pressure was kept at 10%. Therefore, the mixture reference electrode Li_2TiO_3 and TiO_2 can provide constant lithium activity a'_{Li}. The activity calculation at the reference electrode is explained in Appendix A. The lithium activity of the reference side a'_{Li} is 6.77×10^{-22} when O_2 concentration is fixed at 10% at 500°C. For a given O_2 and CO_2 pressure, a''_{Li} is also obtained from the equilibrium reaction occurring at the sensing electrode

$$Li_2CO_3 = 2Li + CO_2 + \frac{1}{2}O_2 \quad [13]$$

The change in the CO_2 partial pressure is then directly related to the change in the lithium activity in the Li_2CO_3 sensing electrode and the measured sensor voltage is expected to follow the Nernst equation (Eq. 11). This calculation is shown in Appendix B. Table VI shows the calculated lithium activity in the Li_2CO_3 sensing electrode and measured emf at 500 and 600°C. Figure 11 shows the phase stability diagram for Li_2CO_3 and other lithium compounds depending on p_{CO_2} and p_{O_2} at 500°C; s indicates the sensor operating region. The dashed line represents the activity of lithium in those compounds. As can be seen, the lithium activity is dependent only on p_{O_2} in the Li_2O and Li_2O_2 region, but it is changed depending on both p_{CO_2} and p_{O_2} in the Li_2CO_3 region. In our experimental condition, a''_{Li} varies from 4.15×10^{-19} (line ①) to 1.31×10^{-20} (line ②) when CO_2 concentration is changed from 500 to 50% with fixed 10% O_2 at 500°C. It shows that Li_2CO_3 is thermodynamically stable and does not decompose at this temperature. Then Li_2O or Li_2O_2 formation is not responsible for the observed deviation from the Nernst equation at 500°C. This is contrary to the studies with Na_2CO_3 electrode,[17-19] explaining the deviation due to the presence of a Na_2O layer. Therefore, it is clear that slow electrochemical reaction or other phase formations is not the main reason for the non-Nernstian behavior of the CO_2 sensor cell at higher than 500°C.

The other possible reason for the emf differences can be a mixed ionic and electronic conduction of Li_3PO_4 electrolyte because ion-conducting ceramics can exhibit partial electronic conduction as temperature increases. If the electrolyte is not a perfect ionic conductor, μ_{Li} and $\tilde{\mu}_{e^-}$ should be defined in the electrolyte based on the local electrochemical equilibrium of Eq. 14, implying that the mass transport of lithium occurs in the electrolyte due to $\Delta\mu_{Li}$ between the sensing and the reference electrode

$$Li^+ + e^- = Li \quad [14]$$

Therefore, the lithium activities at the electrodes are important because the leakage current during mass transport through the electrolyte induces the deviation from the Nernst emf.

If the ionic conductivity (σ_{ion}) or the electronic conductivity (σ_{el}) is not greater than the other by at least two orders of magnitude, then the material is an MIEC.[26] There are three different techniques available in literature to measure the partial electronic or ionic conduction. Tubandt's method[27] is a Faraday transference experiment to measure the mass transport by a dc current equivalent to charge transfer through an electrolyte. Kharton et al. also have used this technique for oxygen conductors such as $LaCo(M)O_3$ (M = Ga, Cr, Fe, or Ni),[29] Bi_2O_3–ZrO_2–Y_2O_3, and Bi_2O_3–NbO_5–H_2O_3.[30] However, this experiment is not suitable for alkali-metal-ion conductors at high temperatures, because it is difficult to measure the accurate mass change of the pure alkali metal electrode and to control the alkali metal activity involving gas–solid interaction.

Näfe et al.[25] reported mixed ionic and p-type conduction in Na -β-alumina based on the emf measurement of a type III sensor with sodium carbonate sensing electrode, and NiO and FeO dissolved in a glass reference electrode. The fact that the Na-β-alumina-based sensor becomes less sensitive at high levels of CO_2 concentration is due to dominant hole conduction in the electrolyte. As the CO_2

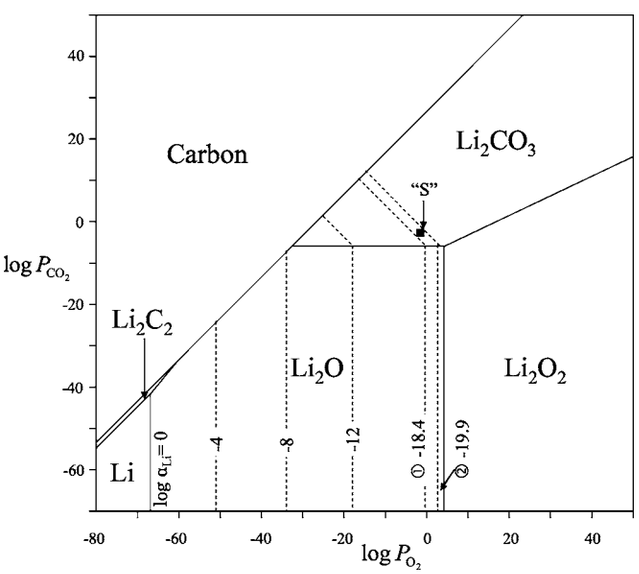

Figure 11. Phase stability diagram for Li_2CO_3 and other lithium compounds with lithium activity depending on p_{CO_2} and p_{O_2} at 500°C.

concentration is increased, sodium activity in the sodium carbonate electrode becomes smaller than the hole conduction parameter, which defines the boundary between the ionic and the hole conduction domains. However, Holzinger et al.[9] observed a Nernstian behavior with Na-β-alumina-based CO_2 sensors under similar CO_2 concentration levels. Therefore, the origin of electronic conduction in the Na-β-alumina and its effects are not completely sorted out.

Wagner[28] developed an experimental technique to measure the transference number by using the dc polarization method, which suppresses either the electronic or ionic conductivity with electron- or ion-blocking electrode. In this study, two techniques, emf measurement and Hebb-Wagner polarization measurement, were used to investigate mixed ionic and electronic conductivity of Li_3PO_4 for a type III CO_2 gas sensor.

Ionic vs electronic conductivity measurement using ion-blocking electrode.— Three polymorphs of Li_3PO_4 (α, β, and γ) are present depending on the temperature: at 520°C ($\beta \rightarrow \gamma$-Li_3PO_4) and 1170°C ($\gamma \rightarrow \alpha$-$Li_3PO_4$).[21] In this study, γ-$Li_3PO_4$ was used as the electrolyte. The transference number of Li_3PO_4 electrolyte has not been reported in literature. Hu et al.[22] studied the conductivity of Li_4SiO_4–Li_3PO_4 solid solution and the individual components. Wang et al.[21] compared the conductivity of pure Li_3PO_4 and $Li_{2.88}PO_{3.73}N_{0.14}$. They used Pt ion-blocking electrodes to measure the ionic conductivity.

Figure 12a shows the equivalent circuit of the ac measurement cell with ion-blocking electrodes. It is assumed that the sample has both ionic and electronic conduction. The ionic resistance (R_i) and the electronic resistance (R_e) are connected in parallel. C_{bl} is the capacitance between Li_3PO_4 and gold-ion-blocking electrode. C_b is the capacitance due to the dielectric property of the solid electrolyte.[31] This equivalent circuit leads to two semicircles with different relaxation times in the impedance plot. At high frequency, ion-blocking electrode cannot block the ionic current, because the impedance of the capacitance component varies reciprocally with the frequency and it is negligible. Therefore, the equivalent circuit can be simplified to three parallel connections of C_b, R_{ion}, and R_{el} (Fig. 12b), but the ionic path is totally blocked by the gold-ion-blocking electrode at low frequencies (Fig. 12c).[32] Hence, it is possible to measure the total conductivity from the high-frequency semicircle and the electronic conductivity from the low-frequency semicircle.

Figure 13 shows a typical impedance spectra using gold-ion-blocking electrodes for different gas concentrations at 500°C. As can be seen, the overall impedance behavior does not change as a function of gas concentration. This indicates that the conduction of Li_3PO_4 electrolyte is chemically stable and insensitive to CO_2 and O_2, justifying the validity of the use of gold as the ion-blocking electrode. AC measurements proved that the total conductivity of Li_3PO_4 is almost equivalent to the ionic conductivity with negligible electronic conductivity when they are attached to the ion-blocking electrode. The measured ionic conductivity can be used for the calculation of the transference number combined with Hebb-Wagner polarization method.

Ionic vs electronic conductivity measurement using reversible electrode.— *EMF measurement method*.— Schmalzried[27,33] derived an analytical expression for determining the ionic transference number from the measured open-circuit voltage of a galvanic cell. Näfe[34,35] applied it to the study of p-type conduction in Na-β-alumina, a sodium ion conductor, assuming that electronic conduction in the oxides is induced by local nonstoichiometry explainable by point defects. Basic assumptions of this method for lithium-ion conductors are (*i*) lithium is the only mobile ion, and ionic defect concentrations are not dependent on μ_{Li}, i.e., ionic conductivity is independent of μ_{Li}, (*ii*) the electron (n-type) and hole (p-type) conductivities are proportional to μ_{Li}, and (*iii*) all conductivities show Arrhenius-type temperature dependence.[26]

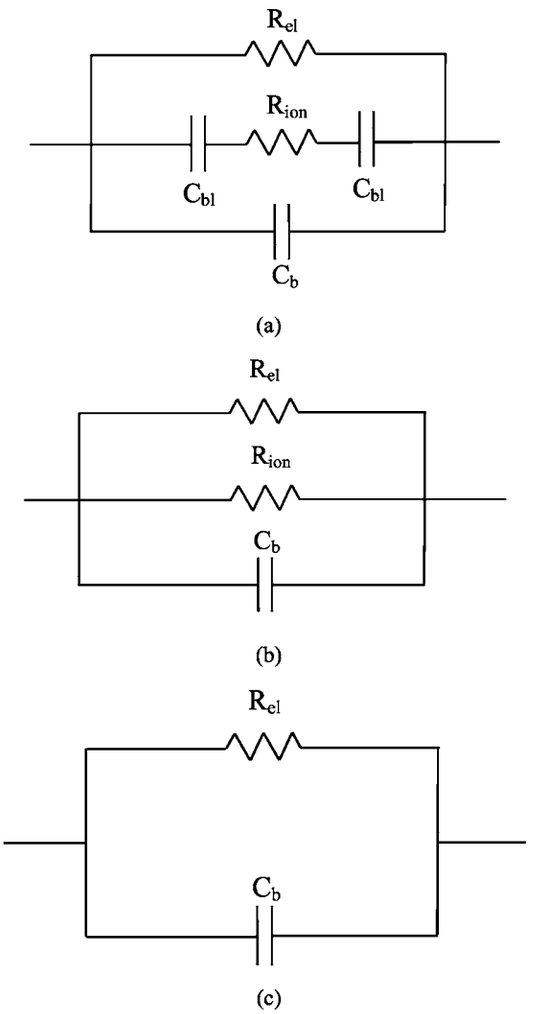

Figure 12. (a) Equivalent circuit of ac measurement cell with ion-blocking electrodes.

The type and extent of intrinsic disorder in the Li_3PO_4 system is not known, and it is reasonable to assume that Frenkel defects of lithium interstititals are predominant. In the stoichiometric composition, the formation of ionic defects in Li_3PO_4 can be represented by the following equilibrium reaction

$$Li_{Li} + V_i = V'_{Li} + Li^{\bullet}_i \qquad [15]$$

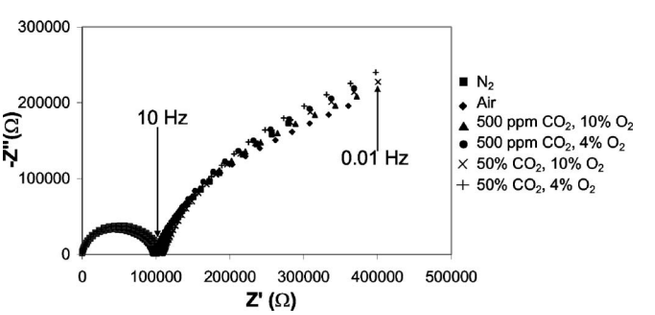

Figure 13. Impedance plot of gold-ion-blocking electrode for Li_3PO_4 under different gas environments at 500°C.

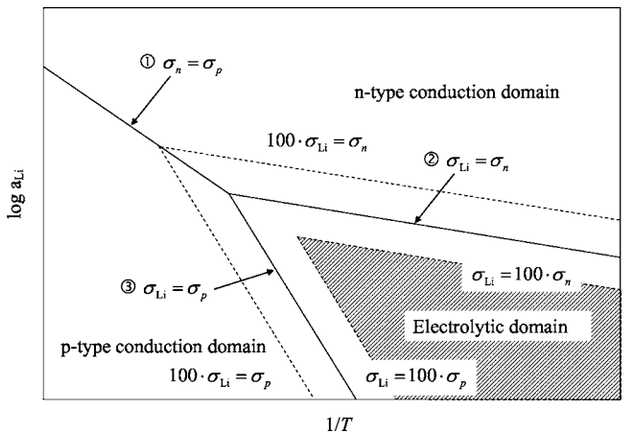

Figure 14. Schematic representation of conduction domain boundaries in log a_{Li} vs $1/T$ space.

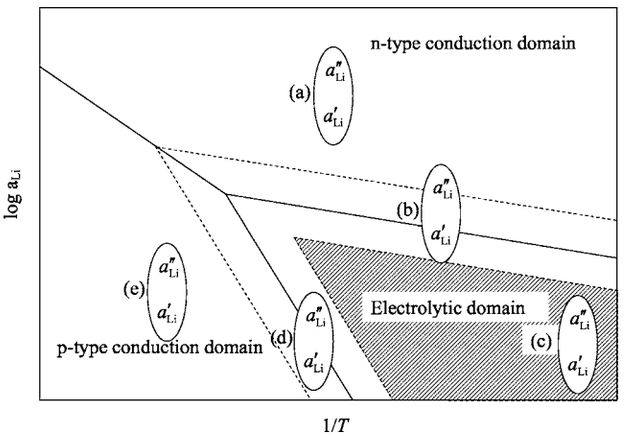

Figure 15. Schematic representation of conduction domain boundaries in log a_{Li} vs $1/T$ space with five different possibilities of sensor operating condition.

$$[V'_{Li}] \approx [Li^{\bullet}_i] = K_F^{-1/2} \quad [16]$$

where K_F is the mass-action constant for Frenkel defect equilibrium. If the a_{Li} at the electrodes is varied, Li_3PO_4 becomes nonstoichiometric due to the Li transport from the Li_2CO_3 to the Li_3PO_4 or the other way around. In these cases, the electron concentration in Li_3PO_4 is directly proportional to a_{Li}, or the hole concentration is inversely proportional to a_{Li} in Li_2CO_3[34]

$$Li_{Li_2CO_3} = Li^{\bullet}_{i,Li_3PO_4} + e'_{Li_3PO_4} \quad [17]$$

$$n = a_{Li} K_F^{1/2} K_n \quad [18]$$

$$Li_{Li_2CO_3} + h^{\bullet}_{Li_3PO_4} = Li^{\bullet}_{i,Li_3PO_4} \quad [19]$$

$$p = a_{Li}^{-1} K_F^{-1/2} K_p^{-1} \quad [20]$$

where K_n and K_p are mass-action constants of electron and hole production in the nonstoichiometric region of Li_3PO_4. For such cases, the partial conductivities of Li_3PO_4 as a function of a_{Li} and temperature are

$$\sigma_{Li^+} = \sigma^o_{Li^+} \exp\left(-\frac{E_{a,Li^+}}{RT}\right) \quad [21]$$

$$\sigma_n = \sigma^o_n a_{Li} \exp\left(-\frac{E_{a\ electron}}{RT}\right) \quad [22]$$

$$\sigma_p = \sigma^o_p a_{Li}^{-1} \exp\left(-\frac{E_{a\ hole}}{RT}\right) \quad [23]$$

where σ^o_j and E_{aj} are the pre-exponential terms and activation energies, respectively, and they are independent of a_{Li} and T. For a given total conductivity ($\sigma_T = \sigma_{Li^+} + \sigma_p + \sigma_n$), the schematic conduction domains of Li_3PO_4 can be represented in the plot of log(a_{Li}) vs $1/T$ space, as shown in Fig. 14. As the lithium activity of the electrode increases at a given temperature, the electronic conduction becomes dominant in the electrolyte, while the hole conduction is significant when the lithium activity decreases. Below the critical temperature (determined by the intersection of the lines ② and ③), the ionic conduction region is located between the electronic and the hole conduction regions. From Eq. 21-23, electron conduction parameter, $a_{\ominus}$ (line ② in Fig. 14) can be determined as a function of the lithium activity where n-type conductivity and ionic conductivity are equal. Similarly, the hole conduction parameter $a_{\oplus}$ (line ③ in Fig. 14) is also calculated. These electron and hole conduction parameters are the material properties of Li_3PO_4 that can be empirically determined. From the definition of MIEC, the electrolytic domain (purely ionic) is smaller than the ionic conduction dominant region between log $a_{\ominus} - 2$ and log $a_{\oplus} + 2$. When the sensor is operated in such a region, the sensor behavior would follow the Nernst equation.

If Li_3PO_4 is not a purely ionic conductor, in other words, the sensor is not operated in the electrolytic domain, the transference numbers should be taken into account to calculate the emf. The ionic transference number, t_j, is defined by the fraction of the ionic conductivity to the total conductivity carried by all charged species[1] and is given by

$$t_j = \frac{\sigma_j}{\sum_j \sigma_j} \quad [24]$$

where σ_j is the conductivity of species j. The electron or hole conductivity is proportional to the ratio of lithium activity at the electrode and electron or hole conduction parameter of Li_3PO_4, respectively, from Eq. 21-23[34]

$$\sigma_n = \sigma_{Li^+} \frac{a_{Li}}{a_{\ominus}} \quad [25]$$

$$\sigma_p = \sigma_{Li^+} \frac{a_{\oplus}}{a_{Li}} \quad [26]$$

From Eq. 25 and 26, the transference number for lithium-ion conduction is represented as a function of lithium activity of the electrode

$$t_{Li^+} = \frac{\sigma_{Li^+}}{\sigma_{Li^+} + \sigma_n + \sigma_p} = \frac{1}{1 + \frac{a_{\oplus}}{a_{Li}} + \frac{a_{Li}}{a_{\ominus}}} \quad [27]$$

The emf of the cell (Eq. 3) can then be calculated by the Wagner equation[28] involving the transference number substituting Eq. 27 into Eq. 28 and integrating

$$\text{emf} = -\frac{1}{F} \int_{\mu'_{Li}}^{\mu''_{Li}} t_{Li^+} \cdot d\mu_{Li} \quad [28]$$

where t_{Li^+} is the Li^+ transference number and μ_{Li} is the chemical potential of Li. Equation 28 leads to the expression shown in Eq. 5. By using this equation, it is possible to calculate the electron conduction parameter or hole conduction parameter from the measured emf and the lithium activity at the sensing and the reference electrodes. Finally, the transference number is calculated from Eq. 27.

When Eq. 5 is used to interpret the measured emf, five different cases can be considered, as shown in Fig. 15. As discussed before,

a''_{Li} is about two orders higher than a'_{Li}, and this relation is described in Fig. 15. Cases (a) and (e) mean that Li_3PO_4 electrolyte shows predominantly electron or hole conduction. In these cases, the emf would approach 0, which is not the case based on the measured values. Case (c) means that both lithium activities reside in the electrolytic domain and the emf should follow the Nernst equation, which is also not the case from the Experimental results. Case (b) means that Li_3PO_4 acts as an MIEC with n-type conduction and ionic conduction, whereas case (d) corresponds to an MIEC with p-type conduction and ionic conduction. Therefore, the current sensor operating condition should resemble either case (b) or case (d). Considering the observed CO_2 sensor behavior, the deviation in the emf from the Nernst equation can be explained by using Eq. 6 and not 7. From multiple sensing tests, it is consistently observed that the emf deviation is more severe at lower CO_2 concentrations (500–5000 ppm) that correspond to higher lithium activities. The measured emf approaches the Nernstian values as the lithium activity is decreased and electronic conduction is minimized. This observation suggests that the decreased CO_2 pressure and hence the increased lithium activity at the sensing electrode makes lithium phosphate nonstoichiometric ($Li_{3+x}PO_4$) with excess lithium, as shown in Eq. 17. Referring to Fig. 15, it seems that the lithium activities on both the electrodes under current sensor operating conditions reside in a conduction regime where n-type electronic conduction is not negligible.

In addition, the second derivatives for Eq. 6 and 7 are, respectively

$$\frac{d^2\text{emf}}{d\ln a''^2_{Li}} = \frac{RT}{F}\frac{a''_{Li}\cdot a_{\ominus}}{(a''_{Li}+a_{\ominus})^2} \quad \text{(for Eq. 6)} \qquad [29]$$

$$\frac{d^2\text{emf}}{d\ln a''^2_{Li}} = -\frac{RT}{F}\frac{a''_{Li}a_{\oplus}}{(a''_{Li}+a_{\oplus})^2} \quad \text{(for Eq. 7)} \qquad [30]$$

The second derivatives have different signs. Consequently, Eq. 6 shows a concave and Eq. 7 a convex variation. Therefore, the fact that the measured emf data with a concave shape can be fitted by Eq. 6 is also an evidence that the deviation from the Nernst equation results from the n-type conduction in Li_3PO_4. Both equations were used to fit the experimental data in Fig. 6 and 7 for comparison. The curve-fitting results confirm that the CO_2 sensor behavior can be explained by the n-type conduction in Li_3PO_4 ionic conductors.

The electronic conduction parameter, $a_{\ominus}$, and the lithium activity, a'_{Li}, are obtained from the curve-fitting by Eq. 6. The estimated value of a'_{Li} was used to calculate $\mu^{o}_{Li_2TiO_3}$ using Eq. A-4 and was found to be 1424.6 kJ at 500°C. This value is in good agreement with the literature value of 1430.6 kJ,[23] measured by solution calorimetry. The electronic conduction boundary is represented in Fig. 16 from the electronic conduction parameter $a_{\ominus}$ in Table IV. The electronic conduction parameter is a function of temperature on the $\log a_{Li}$ vs $10000/T$ plane and is given by

$$\log a_{\ominus} = -1.810\left(\frac{10000}{T}\right) + 5.403 \qquad [31]$$

As can be seen from Fig. 16, the lithium activities at the sensing electrode are located in the n-type conduction region, slightly above the electron conduction parameter where Li_3PO_4 shows the mixed ionic and electronic conduction behavior. On the contrary, the lithium activity at the reference electrode is lower by 2 orders of magnitude than the electronic conduction parameter in which purely ionic conduction prevails. Transference numbers were calculated from the electronic conduction parameters and the lithium activities at the electrodes by using Eq. 27 when Li_2CO_3 is in contact with a Li_3PO_4 ionic conductor. These results are shown in Fig. 17. Generally, the ionic transference numbers at 500°C are higher than those at 600°C, and they also increase with the CO_2 partial pressure due to the decreased lithium activities at all temperatures.

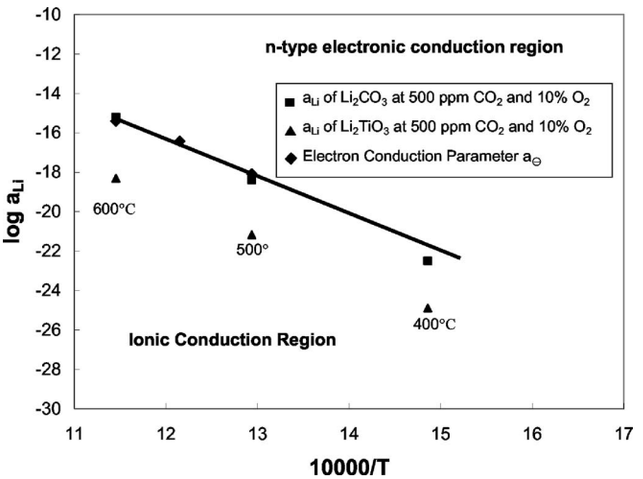

Figure 16. Electronic conduction parameter calculated from the emf measurement and the lithium activity at the measuring and reference electrodes at 400, 500, and 600°C.

Hebb-Wagner polarization measurement.— For the study of mixed ionic and electronic conduction in the current sensor structure, Li_2CO_3 and gold mixture was used as a reversible electrode. Figure 18 shows the schematic design and chemical and electrical potential profiles of the cell.[8] Li_2CO_3 and gold mixture provide the relation, $\tilde{\mu}_{e-,Au\prime} = \tilde{\mu}_{e-,Li_2CO_3}$. Initial current must be the mixed ionic and electronic current due to the migration of lithium ion from the ion-blocking electrode (gold) to the reversible electrode (Li_2CO_3 + gold), but only electron or hole conduction plays a role in the steady-state current under the polarization condition. Therefore, it is assumed that $\Delta\tilde{\mu}_{Li^+,Li_3PO_4} = 0$ is established in Li_3PO_4 because there is no Li-ion transport. The chemical potential gradient of $\Delta\mu_{Li,Li_3PO_4}$ in Li_3PO_4 results in the $\Delta\tilde{\mu}_{e-,Li_3PO_4}$ due to the electrochemical equilibrium, $\Delta\tilde{\mu}_{e-,Li_3PO_4} + \Delta\tilde{\mu}_{Li^+,Li_3PO_4} = \Delta\mu_{Li,Li_3PO_4}$ from Reaction 14 and $\Delta\tilde{\mu}_{Li^+,Li_3PO_4} = 0$. Therefore, electronic conduction with polarized condition is established by chemical potential gradient of neutral species rather than electrical potential gradient. Ionic defect concentration is predominant in Li_3PO_4, and it is not changed under

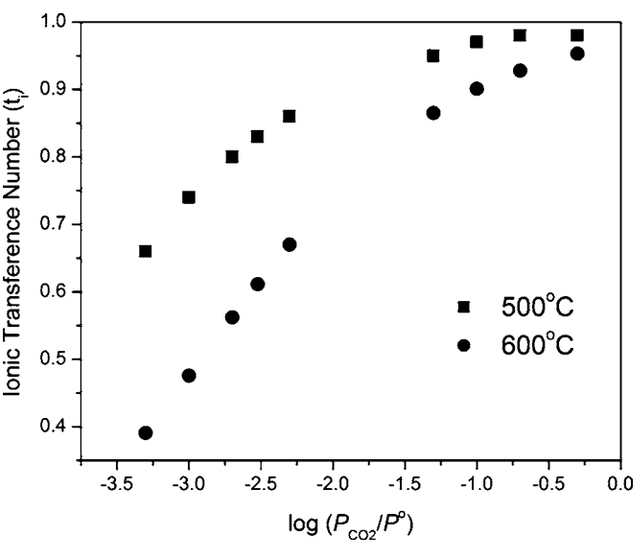

Figure 17. Ionic transference number calculated from the measured emf and the electronic conduction parameter under various p_{CO_2} at 500 and 600°C.

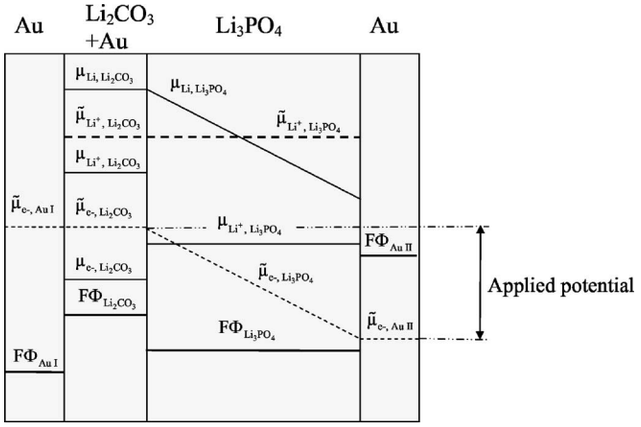

Figure 18. Schematic profile of electrochemical, chemical, and electrical potentials of the Hebb-Wagner cell with an MIEC.

polarization except for the region where Li_3PO_4 is close to the ion-blocking electrode. This small region is responsible for most of the potential drop in this applied field, and there is no electrical potential gradient in Li_3PO_4 based on Wagner's theory.[28] Hebb[36] showed experimentally that potential drop in Ag_2S with ion-blocking electrodes was 0.2 V when 1.5 V was applied between two electrodes of Ag_2S.

The $[1 - \exp(-EF/RT)]$ term in Eq. 10 becomes unity when the applied voltage is higher than 0.2 V at 500°C. So if σ_n is not as large as σ_p, the current density is only determined by the hole conductivity, which shows an exponential function, $\sigma_p[\exp(EF/RT) - 1](RT/FL)$. If σ_n is larger than σ_p, the current density saturates to the value of $\sigma_n(RT/FL)$. As shown in Fig. 9, the I-V curve of the cell (Eq. 8) shows the plateau current between 0.3 and 0.9 V, which represents an n-type electronic conduction behavior rather than a p-type. The increase in current above 0.9 V at 500°C might be due to hole conduction or decomposition of the sample. The ionic transference numbers were calculated from the equation

$$t_{Li^+} = \frac{\sigma_{Li^+}}{\sigma_{Li^+} + \sigma_n + \sigma_p} \qquad [32]$$

where the result with ion-blocking electrode in the previous discussion was used for the ionic conductivity, σ_{Li^+}, because it is assumed that σ_{Li^+} is not changed depending on lithium activity. σ_n and σ_p are obtained from the fit of the experimental data as shown in Fig. 9. The Hebb-Wagner polarization measurement shows similar transference numbers at 500 and 600°C (Table VII), but the emf measurement shows lower ionic transference numbers at 600°C. In literature,[27,37,38] two possibilities of experimental errors for Hebb-Wagner polarization measurements are discussed. When samples decompose, measured steady-state current represents not only the electronic but also the ionic current, which is controlled by the decomposition rate. However, if the decomposition current is included in the measured current, the measured electronic conductivity should be higher than the true electronic conductivity, which results in a lower lithium-ion transference number from Hebb-Wagner polarization measurements. Ion-blocking electrode must block only the ionic transport in this measurement. If ion-blocking electrode induces the polarization of electrons, it could decrease the electronic current. In this case, measured current is determined by the Li chemical potential gradient in the Li_3PO_4, as well as the polarization resistance at the interface between Li_3PO_4 and gold-ion-blocking electrode. Therefore, it is more probable that our Hebb-Wagner polarization measurement might have reduced the electronic current due to the polarization of electrons at the ion-blocking electrode. In spite of the difference between two different transference number measurements, it is clear that the electronic conductivity is significant when Li_2CO_3 is attached to the Li_3PO_4 electrolyte from these experiments.

Conclusions

The total conductivity measured with gold-ion-blocking electrode from the ac measurement agrees well with the values reported in literature. Li_3PO_4 is a purely ionic conductor when it is used in contact with ion-blocking electrode, and therefore, the total conductivity is practically the same as the ionic conductivity. The electron conduction parameters calculated from the emf measurement with Li_2CO_3 sensing electrode and Li_2TiO_3 reference electrode describe the conduction regime of Li_3PO_4 near the boundary between the n-type and the ionic conduction region. The emf measurement showed that the lithium activity of Li_2CO_3 sensing electrode is located in the mixed n-type and ionic conduction region of Li_3PO_4, but the lithium activity at the reference electrode is in the electrolytic region. Above 500°C, the Hebb-Wagner dc polarization measurement also shows significant n-type conduction when Li_3PO_4 is in contact with Li_2CO_3 sensing electrode. This result combined with the emf measurement suggests that the current Li_3PO_4 electrolyte possesses significant electronic conduction when Li_2CO_3 is used as the sensing electrode. The nonstoichiometric composition of Li_3PO_4 due to the mass transport of Li from the Li_2CO_3 electrode to the Li_3PO_4 electrolyte is responsible for the electronic conduction in the CO_2 sensor.

Acknowledgment

This work was supported by CISM through National Science Foundation contract no. EEC-9523358, U.S. Department of Energy contract no. DE-FC26-03NT41615, and NASA-GMI contract no. NNC04AA48A.

The Ohio State University assisted in meeting the publication costs of this article.

Appendix A

Reference Electrode Reaction

From Reaction 12, we have

$$\mu_{Li_2TiO_3} = 2\mu_{Li} + \mu_{TiO_2} + \frac{1}{2}\mu_{O_2} \qquad [A\text{-}1]$$

Expanding, we have

$$\mu^o_{Li_2TiO_3} + RT\ln a_{Li_2TiO_3} = 2(\mu^o_{Li} + RT\ln a_{Li}) + \mu^o_{TiO_2} + RT\ln a_{TiO_2} + \frac{1}{2}(\mu^o_{O_2} + RT\ln p_{O_2}) \qquad [A\text{-}2]$$

where $a_{Li_2TiO_3} = 1$, $a_{TiO_2} = 1$, $\mu^o_{Li} = 0$, and $\mu^o_{O_2} = 0$

Table VII. Ionic conductivity, electronic conductivity, hole conductivity, and ionic transference number calculated from the Hebb-Wagner (HW) method and the emf measurement at 500 and 600°C.

Temp (°C)	Ionic conductivity (S cm^{-1})	Electronic conductivity measured from HW (S cm^{-1})	Hole conductivity measured from HW (S cm^{-1})	t_i (measured by HW)	t_i (measured by emf method)
500	5.58×10^{-6}	5.34×10^{-6}	3.62×10^{-14}	0.51	0.66
600	4.83×10^{-5}	4.80×10^{-5}	4.36×10^{-15}	0.50	0.39

$$\mu^{o}_{Li_2TiO_3} = 2RT \ln a'_{Li} + \mu^{o}_{TiO_2} + \frac{1}{2}RT \ln p_{O_2} \quad [A\text{-}3]$$

The lithium activity at the reference electrode is

$$a'_{Li} = \exp\left[\frac{\mu^{o}_{Li_2TiO_3} - \mu^{o}_{TiO_3}}{2RT} - \frac{1}{4}\ln p_{O_2}\right] \quad [A\text{-}4]$$

Appendix B
Sensing Electrode Reaction

From Eq. 13 we have

$$\mu_{Li_2CO_3} = 2\mu_{Li} + \mu_{CO_2} + \frac{1}{2}\mu_{O_2} \quad [B\text{-}1]$$

Expanding, we obtain

$$\mu^{o}_{Li_2CO_3} + RT \ln a_{Li_2CO_3} = 2(\mu^{o}_{Li} + RT \ln a_{Li}) + \mu^{o}_{CO_2} + RT \ln p_{CO_2} + \frac{1}{2}(\mu^{o}_{O_2} + RT \ln p_{O_2}) \quad [B\text{-}2]$$

where $a_{Li_2CO_3} = 1$, $\mu^{o}_{Li} = 0$, and $\mu^{o}_{O_2} = 0$

$$\mu^{o}_{Li_2CO_3} = 2RT \ln a''_{Li} + \mu^{o}_{CO_2} + RT \ln p_{CO_2} + \frac{1}{2}RT \ln p_{O_2} \quad [B\text{-}3]$$

Thus, we arrive at

$$a''_{Li} = \exp\left[\frac{\mu^{o}_{Li_2CO_3} - \mu^{o}_{CO_2}}{2RT} - \frac{1}{4}\ln p_{O_2} - \frac{1}{2}\ln p_{CO_2}\right] \quad [B\text{-}4]$$

References

1. C. Park and S. Akbar, *J. Mater. Sci.*, **38**, 4639 (2003).
2. W. Weppner, *Solid State Ionics*, **1992**, 29.
3. N. Yamazoe and N. Miura, *J. Electroceram.*, **4**, 243 (1998).
4. J. Maier, *Sens. Actuators B*, **65**, 199 (2000).
5. M. Gauthier and A. Chamberland, *J. Electrochem. Soc.*, **124**, 1579 (1977).
6. J. Liu and W. Weppner, *Solid State Ionics*, **1992**, 61.
7. N. Miura, S. Yao, Y. Shimizu, and N. Yamazoe, *J. Electrochem. Soc.*, **139**, 1384 (1992).
8. Y. Sadaoka, Y. Sakai, M. Matsumoto, and T. Manabe, *J. Mater. Sci.*, **28**, 2035 (1993).
9. M. Holzinger, J. Maier, and W. Sitte, *Solid State Ionics*, **86–88**, 1055 (1996).
10. C. Lee, S. A. Akbar, and C. O. Park, *Sens. Actuators B*, **80**, 234 (2001).
11. C. O. Park, C. Lee, S. A. Akbar, and J. Hwang, *Sens. Actuators B*, **88**, 53 (2003).
12. N. Szabo, C. Lee, J. Trimboli, O. Figueroa, R. Ramamoorthy, S. Midlam-Mohler, A. Soliman, H. Verweij, P. Dutta, and S. Akbar, *J. Mater. Sci.*, **38**, 4239 (2003).
13. O. L. Figueroa, C. Lee, S. A. Akbar, N. F. Szabo, J. A. Trimboli, P. K. Dutta, N. Sawaki, A. A. Soliman, and H. Verweij, *Sens. Actuators B*, **107**, 839 (2005).
14. J. B. Bates, N. J. Dudney, D. C. Lubben, G. R. Gruzalski, B. S. Kwak, X. Yu, and R. A. Zuhr, *J. Power Sources*, **54**, 58 (1995).
15. B. Wang, J. B. Bates, F. X. Hart, B. C. Sales, R. A. Zuhr, and J. D. Robertson, *J. Electrochem. Soc.*, **143**, 3203 (1996).
16. X. Yu, J. B. Bates, G. E. Jellison, and F. X. Hart, *J. Electrochem. Soc.*, **144**, 524 (1997).
17. Y. Sadaoka, Y. Sakai, and T. Manabe, *Sens. Actuators B*, **13–14**, 532 (1993).
18. M. Alonso-Porta and R. V. Kumar, *Sens. Actuators B*, **71**, 173 (2000).
19. J. Ramirez-Salgado and P. Fabry, *Solid State Ionics*, **158**, 297 (2003).
20. C. Lee, Ph.D. Dissertation, The Ohio State University, Columbus, OH (2004).
21. B. Wang, B. C. Chakoumakos, B. C. Sales, B. S. Kwak, and J. B. Bates, *J. Solid State Chem.*, **115**, 313 (1995).
22. Y. Hu, I. D. Raistrick, and R. A. Huggins, *J. Electrochem. Soc.*, **124**, 1240 (1977).
23. M. W. Chase, Jr., *NIST-JANAF Thermochemical Tables*, 4th ed. (1998).
24. C. Lee, N. Szabo, R. Ramamoorthy, P. Dutta, and S. Akbar, in *Encyclopedia of Sensors*, C. A. Grimes and E. C. Dickey, Editors, American Scientific Publishers, Stevenson Ranch, CA, In press.
25. H. Näfe, S. Gollhofer, and F. Aldinger, *J. Electrochem. Soc.*, **149**, E311 (2002).
26. J. W. Patterson, *J. Electrochem. Soc.*, **118**, 1033 (1971).
27. R. A. Rapp, *Tech. Met. Res.*, **4**, 123 (1970).
28. C. Wagner, in *Proceedings of the 7th Meeting of the International Committee on Electrochemical Thermodynamics and Kinetics*, Lindau 1955, p. 361, Butterworths Scientific, London (1957).
29. V. V. Kharton, A. P. Viskup, E. N. Naumovich, and N. M. Lapchuk, *Solid State Ionics*, **104**, 67 (1997).
30. A. A. Yaremchenko, V. V. Kharton, E. N. Naumovich, A. A. Tonoyan, and V. V. Samokhval, *J. Solid State Electrochem.*, **2**, 308 (1998).
31. J. R. Macdonald, *Impedance Spectroscopy-Emphasizing Solid Materials and Systems*, John Wiley & Sons, New York (1987).
32. V. Thangadurai, R. A. Huggins, and W. Weppner, *J. Power Sources*, **108**, 64 (2002).
33. H. Schmalzried, *Chemical Kinetics of Solids*, p. 374, VCH, New York (1995).
34. H. Näfe and M. Steinbrück, *J. Electrochem. Soc.*, **131**, 2779 (1994).
35. H. Näfe, *J. Electrochem. Soc.*, **143**, 943 (1996).
36. M. H. Hebb, *J. Chem. Phys.*, **20**, 185 (1952).
37. I. Riess and H. L. Tuller, *Solid State Ionics*, **72**, 3 (1994).
38. W. Weppner and R. A. Huggins, *Annu. Rev. Mater. Sci.*, **8**, 269 (1978).